Electroconvection in freely suspended smectic-*C* and smectic-*C** films

C. Langer and R. Stannarius
Universität Leipzig, Fakultät für Physik und Geowissenschaften, Linnéstrasse 5, 04103 Leipzig, Germany
(Received 19 December 1997)

Electrohydrodynamic convection in freely suspended smectic-*C* (S_C) and smectic-*C**(S_C^*) films is investigated experimentally by means of reflection polarizing microscopy. A two-dimensional vortex flow is observed when a dc field is applied in the plane of the smectic layers while the electrodes are in contact with the film. Measurements of the threshold voltage, the vortex velocity, and the vortex pattern wavelength are presented. In S_C films the convection is driven by the interaction of the applied electric field with space charges at the free surfaces of the films. The threshold voltage depends on the conductivity and is linearly related to the film thickness. Convective flow can be visualized directly from the optical textures. In S_C^* films the threshold voltage is close to zero and the flow velocity is rather independent of film thickness, suggesting that bulk charges drive the convection. [S1063-651X(98)12107-4]

PACS number(s): 61.30.−v

INTRODUCTION

Electroconvection effects in liquid crystals represent useful models for dissipative pattern formation as they can be easily studied in experiments and provide convenient time scales and reasonable aspect ratios. In particular, the variable degree of complexity from an isotropic material to ordered nematic and smectic liquid crystalline phases makes these systems attractive to basic studies of pattern formation processes. Well-known standard systems are nematic liquid crystals confined between glass plates that have been studied intensively both theoretically and experimentally. A recent review is given, for example, in [1]. The onset of convection is explained by the Carr-Helfrich mechanism, which is based on an anisotropic conductivity [4]. A few experiments on electrohydrodynamic instabilities in S_C and S_C^* sample cells have been reported in the past (see [2,3] and references therein). All types of electroconvection are driven by the interaction of an external electric field with an inhomogeneous space charge density. Thus, the mechanisms leading to electroconvection depend on the formation of unstable space charge density distributions.

Freely suspended films represent macroscopically oriented samples with perfectly stacked layers. Due to their geometrical dimensions and the restriction of the hydrodynamic flow to the film plane, they can be considered as quasi-2D systems. Previous electro-optic experiments in S_C and S_C^* films exposed to rotating electric fields have been reported, for example, in [5,6], where spiral and target patterns have been observed. Maclennan [7] observed electric field instabilities and convective flow pattern in ferroelectric S_C^* films.

In S_C and S_C^* films, different possible electroconvection mechanisms have to be taken into account. One is the Carr-Helfrich effect, which for S_C and S_C^* films has been predicted theoretically by Ried *et al.* [8] but has not yet been confirmed in experiment. On the other hand, a vortex mode instability that was studied before in smectic-*A* [9–11] and nematic films [12,13] was recently observed in S_C films too [14]. This type of convection is driven by surface charges interacting with the electric field. Another possible mechanism is based on charge injection from nonisolating electrodes. This mechanism has been observed in nonconducting dielectric liquids confined between capacitor plates [15–17]. An early description of a vortex flow based on charge injection in a capacitor filled with dielectric liquids was given by Avsec and Luntz [18].

Faetti *et al.* [12,13] first reported about electroconvection in freely suspended liquid crystal films. In their experiments with unstable nematic and isotropic films they observed a convection type independent of the anisotropic properties of the liquid crystal which they called ''vortex mode'' [12]. The onset voltage of this vortex mode linearly depended on the film thickness, indicating a surface charge effect. As coating of the electrodes with isolating paint had no effect on the convection, charge injection mechanisms as reported in [15] were excluded. Faetti *et al.* claimed that the onset of convection is caused by an inhomogeneous space charge density at the free surfaces of the film and proposed a simple surface charge model that predicts a linear relation between the threshold voltage U_c and the film thickness s [12]. They also found a ''domain mode'' for thick nematic films ($s \geqslant 7 \pm 3\,\mu$m) that was interpreted in terms of the Carr-Helfrich mechanism [13]. However, as in the absence of a smectic layer structure the hydrodynamic flow field causes thickness variations of the film, the quantitative analysis of nematic films is quite complicated. As nematic films are unstable, they are not suitable for intensive research, so there has been practically no further progress in this field.

Morris *et al.* [9,10] and Mao *et al.* [11] performed experiments on stable smectic-*A* liquid crystal films freely suspended between two wire electrodes. The smectic-*A* phase is organized in layers where the average molecular orientation is normal to the layer plane. In the S_A films, a two-dimensional vortex mode instability similar to the nematic vortex mode was observed. Again, the onset of convection occurred above a well-defined threshold voltage U_c, which turned out to be linearly related to the film thickness. Near the onset of convection the periodicity λ of the vortex pat-

tern was approximately 1.3 times the electrode distance d. A linear stability analysis for dc voltages and the film geometries used in [9–11] was carried out by Daya *et al.* [19] and recently extended to a weakly nonlinear analysis [20]. The results of these theoretical calculations, which are based on the surface charge model, showed qualitatively good agreement with the threshold voltages estimated experimentally. The measured dc λ values were quantitatively confirmed.

First experiments on S_C films [14] showed vortex flow convection coupled with a reorientation of the c director. The smectic-C phase is optically anisotropic in the layers, as the preferred molecular orientation is tilted with respect to the layer normal. In a polarizing microscope this anisotropy allows direct optical observation of the flow that induces characteristic director patterns. Our objective is to perform quantitative electroconvection experiments in S_C films and to extend it to ferroelectric S_C^* films where an additional coupling between the electric field **E** and the spontaneous polarization $\mathbf{P}_s$ has to be taken into account. We will show that this leads to significant differences between S_C and S_C^* films: The interactions between the director field and flow field cause different optical effects, and the convection mechanism seems to be remarkably modified by the polar interaction.

In addition to the phenomena described for S_A films, the in-plane anisotropy in the S_C or S_C^* phase allows in principle electroconvection of the Carr-Helfrich (CH) type, which is based on an anisotropic conductivity. Due to the tilt in the S_C and S_C^* films, the in-plane anisotropy in combination with small c-director fluctuations induces regions of opposite space charge within the smectic layers, which above a certain threshold field may generate electroconvection domains. A theoretical analysis of CH electroconvection in S_C and S_C^* films was carried out by Ried *et al.* [8], without taking into account the surface charge mechanism and the finite film thickness. Describing the film with a two-dimensional theory, regimes of the conductive and dielectric instability type similar to those observed in nematic liquid crystals were found from linear stability analysis. Ried *et al.* pointed out that the CH effect competes with a director reorientation instability due to the generalized Fredericks transition. This restricts the parameter ranges where CH electroconvection can be observed experimentally.

EXPERIMENTAL SETUP

Our experiments are performed on smectic films freely suspended between two movable and two fixed holders [Fig. 1(b)]. Well-controlled films of homogeneous thickness are drawn in the smectic-A phase by putting the movable holders together, spreading some amount of the smectic liquid crystal substance on their edges, and then carefully tearing the holders apart. The film width is given by the distance between the fixed holders, which is about 6 mm, while the film length can be varied from 0 to 7 mm. The film holders are contained in a heating stage and the films can be stabilized at a given temperature to ± 0.1 K.

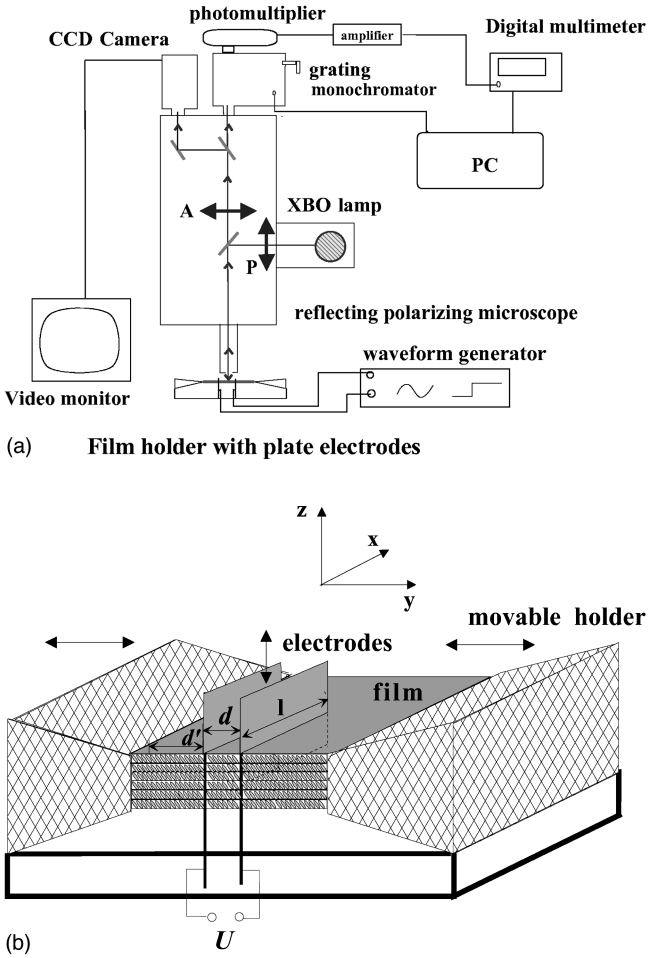

FIG. 1. (a) Schematic drawing of the experimental setup. (b) Film holder with electrodes: The smectic film is suspended between two movable and two fixed holders. In the picture, only the movable holders are sketched. Two parallel microplate electrodes are pierced into the film.

We have studied one enantiomorphic and one nonenantiomorphic substance. The S_C^* films are made of the chiral mixture ZLI 4237-100 (Merck) [21]. The S_C substance investigated is a 1:1 mixture of *5-n-octyl-2-(4-n-hexyloxyphenyl)-pyrimidin* and *5-n-octyl-2-(4-n-octyloxyphenyl)-pyrimidin*. The two substances show the following phase transition sequences:

S_C mixture (Weissflog, Halle):	$\xleftrightarrow[-10\,^\circ\mathrm{C}]{}$	S_C	$\xleftrightarrow[50.5\,^\circ\mathrm{C}]{}$	S_A	$\xleftrightarrow[53\,^\circ\mathrm{C}]{}$	N	$\xleftrightarrow[68\,^\circ\mathrm{C}]{}$	I
S_C^* mixture ZLI 4237-100:	$\xleftrightarrow[-20\,^\circ\mathrm{C}]{}$	S_C^*	$\xleftrightarrow[61\,^\circ\mathrm{C}]{}$	S_A	$\xleftrightarrow[73\,^\circ\mathrm{C}]{}$	N*	$\xleftrightarrow[83\,^\circ\mathrm{C}]{}$	I

All electroconvection measurements in the S_C or S_C^* phase were performed near room temperature (25 °C) far below the transition to S_A. After the film has been brought to thermal equilibrium, two parallel microelectrode plates with distance $d=500$ μm are carefully pierced into the film. The electrode length l is about 2.5 mm providing a reasonable aspect ratio l/d of 5. In the experiments, dc and low frequency ac voltages are applied between the electrodes. Some experiments with higher aspect ratios have been performed by applying the voltage between the drawing edge and one electrode, which allowed a continuous variation of the distance d' [Fig. 1(b)]. If d' is smaller than ≈ 500 μm, the field between electrode and holder is practically homogeneous.

Observations of the films were carried out with polarized light using a Carl-Zeiss-Jena NU2 reflection polarizing microscope [Fig. 1(a)]. The transmission images were recorded with a HAMAMATSU charge-coupled device camera connected to a C2400 camera controller for contrast enhancement.

The film thickness is measured by means of reflection spectroscopy [22]. For this purpose, a grating monochromator connected with a photomultiplier is mounted on the microscope. After passing the analyzer and monochromator, the reflected light is detected by a photomultiplier, amplified, digitized, and processed in a computer.

OPTICS AND ORIENTATION

The S_C and S_C^* phases are organized in layers where the average molecular orientation **n** is tilted at an angle θ relative to the layer normal. The projection of **n** onto the layer plane is the c director **c**. The chiral S_C^* phase shows an additional intrinsic twist of the c director from layer to layer in the bulk phase and a spontaneous electric polarization $\mathbf{P}_s$ in the layer planes perpendicular to **c** (Fig. 2). The pitch p is defined as the periodicity of the c director along the layer normal. For the ZLI 4237-100 mixture, the pitch is about 10 μm at 20 °C [21], which is always much larger than the film thickness in our experiments.

In the presence of an electric field **E**, the polarization $\mathbf{P}_s$ tends to align parallel to the field, such that the c director will be aligned parallel to the electrode planes. Dielectric interactions with the external field, due to the nonzero effective in-plane anisotropy $\Delta\epsilon$, are negligibly small in both S_C and S_C^* phases. The tilted smectic layers are optically biaxial. However, this biaxiality is so small that the S_C layers can be treated as uniaxial, with the preferred molecular direction **n** as the optical axis. When the film is observed at normal incidence, two refractive indices in the film plane are effective. If the refractive indices perpendicular and parallel to **n** are given by n_o and n_e, respectively, the effective refractive index for polarization parallel to the orientation of **c** is

$$n_1=\frac{n_o n_e}{\sqrt{(n_e^2\cos^2\theta+n_o^2\sin^2\theta)}} \tag{1}$$

while in the orthogonal direction the refractive index is n_o. The local orientation of the c director can be detected in reflected polarized light incident normal to the layer, as the reflected intensity is a function of the angle α between the c director and the polarizer. Contrast variations in the reflection texture of the film indicate a nonuniform c-director field (Fig. 3).

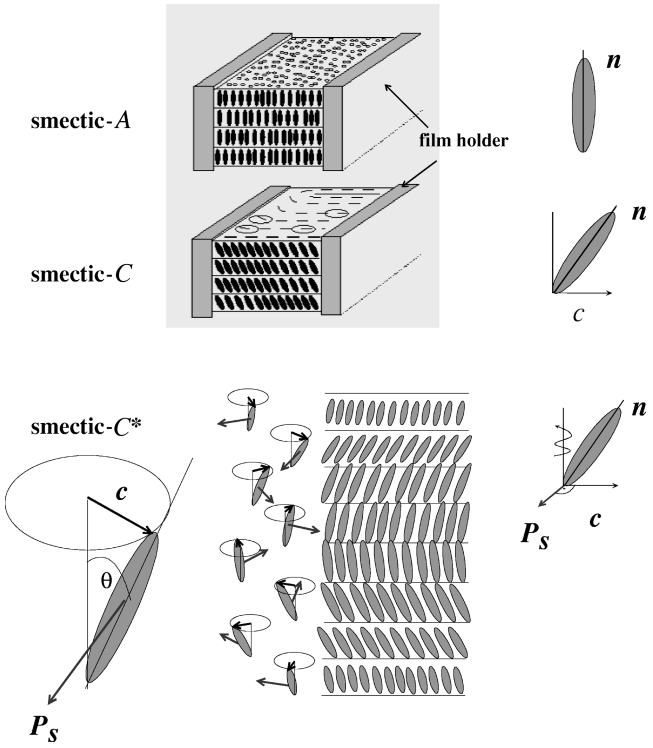

FIG. 2. Schematic drawing of molecular orientation in S_A, S_C, and S_C^* films. **n** is the average molecular orientation; the projection of **n** on the layer plane is the c director **c**, giving the azimuthal orientation of **n**. Θ is the tilt with respect to the layer normal. $\mathbf{P}_s$ denotes the vector of the spontaneous polarization.

The reflectivity $R(\alpha)$ can be calculated from the sum of directly and multiply reflected light beams [6,23]. For crossed polarizers, $R(\alpha)$ is

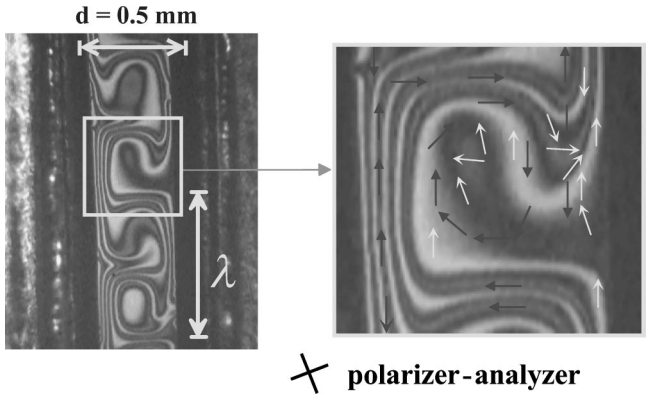

FIG. 3. Vortex flow electroconvection in a smectic-C film above the threshold voltage $U_c=10.75$ V at a dc voltage $U=60$ V. The film thickness s is 2493 nm. The pattern wavelength λ is defined as the lateral periodicity of the flow field, which consists of pairs of counter-rotating vortices. The c-director field winds up due to advection with the hydrodynamic flow, leading to a texture of spirals and concentric rings that indicate disclination walls. In the enlarged area, dark arrows mark the flow field while bright arrows symbolize the c-director field.

$$R(\alpha)=(\sin^2\alpha)(\cos^2\alpha)[|\psi_1|^2+|\psi_o|^2-(\psi_1\psi_o^*+\psi_o\psi_1^*)], \tag{2}$$

where

$$\psi_{1,o}=r_{1,o}\frac{1-e^{2i\phi_{1,o}}}{1-r_{1,o}^2e^{2i\phi_{1,o}}}$$

and

$$\phi_{1,o}=\frac{2\pi}{\lambda}n_{1,o}s, \quad r_{1,o}^2=\frac{(n_{1,o}-1)^2}{(n_{1,o}+1)^2}.$$

The indices o,1 correspond to the two eigenmodes in the LC layers. The ψ term in brackets is determined by the phase difference between ordinary and effective extraordinary light, which is usually very weak in thin films. Typical ordinary and extraordinary refractive indices are 1.5 and 1.65, respectively. For example, if we take these standard values and the tilt angle $\Theta=23.5°$ for the ZLI 4237-100 mixture [21], we obtain an optical anisotropy $n_1-n_o=0.02$. Then, the order of interference $2(n_1-n_o)d/\lambda$ is only 0.1 even for a 2.5 μm film. The periodicity of the optical intensity varies with $\sin4\alpha$, that is, subsequent bright and dark regions in the images mark domains that differ by 45° in the c-director orientation.

In the case of parallel polarizers, the reflectivity is

$$R(\alpha)=(\cos^4\alpha)|\psi_1|^2+(\sin^4\alpha)|\psi_o|^2 +(\sin^2\alpha)(\cos^2\alpha)(\psi_1\psi_o^*+\psi_o\psi_1^*). \tag{3}$$

The intensity modulation for thin films ($s\ll1\mu$m) is determined by the different reflection coefficients r_1,r_o for light polarized parallel and perpendicular to **c**, and the periodicity of optical contrast is $\sin2\alpha$. However, this intensity is superimposed by a large background signal (reflection from below the film). Therefore we have used crossed polarizers in most experiments. The orientation of the c director influences the interference curve only marginally. However, the c-director orientation can be detected by means of the contrast enhancement facilities of the camera controller. Using the crossed polarizer-analyzer position, we obtain very sharp contrast images on the video screen.

For the film thickness determination in the S_C and S_C^* phases, the well-known complementary Airy function resulting from Eq. (3) for $n_1=n_o$,

$$\frac{I(\lambda)}{I_0}=\frac{f\sin^2(2\pi n_o s/\lambda)}{1+f\sin^2(2\pi n_o s/\lambda)}, \quad f=\frac{(n_o^2-1)^2}{4n_o^2}, \tag{4}$$

can be applied in order to determine n_o and the thickness s. Strictly, this equation holds only for films that are optically isotropic in the layer plane, so it requires measurements in the S_A phase at higher temperatures. However, for film thickness determination in the S_C or S_C^* phase we can approximately treat the film as in-plane isotropic like and determine n_o and s from Eq. (4). The error in the thickness determination is less than $(n_1-n_o)/n_o\approx2\%$, which is negligible for our purposes.

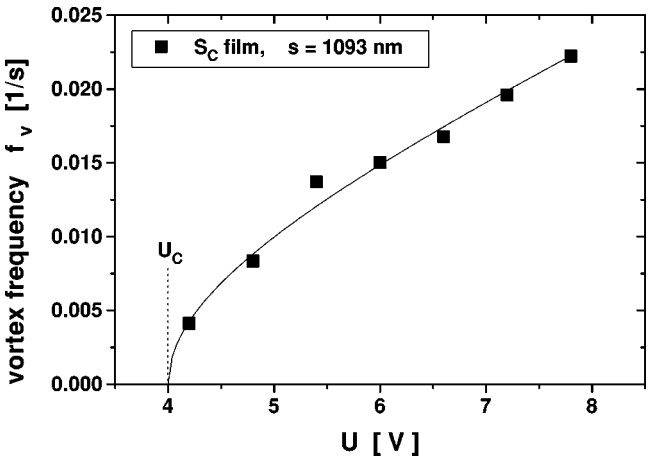

FIG. 4. Example of a vortex frequency plot for a 1093 nm S_C film. The vortex frequency f_v was measured as a function of the voltage applied. The solid curve is a fit to $f\propto[(U^2-U_c^2)/U_c]^{1/2}$ with $U_c=4$ V.

In this way we have measured values $n_o=1.475$ for ZLI 4237-100 and $n_o=1.424$ for the smectic-C mixture at 25 °C.

ELECTROCONVECTION MEASUREMENTS

The general scenario of electroconvective pattern formation in the smectic films is as follows: When a sufficiently large dc voltage is applied to the electrodes, a periodic flow pattern consisting of pairs of alternating vortices sets in as shown in Fig. 3. With increasing voltage, the vortex rotation velocity increases and the vortices become more and more pronounced. At even higher voltages, the vortices become unstable as the flow becomes irregular.

The hydrodynamic flow in the vortices can be visualized in several ways: The simplest way proposed in the literature is the observation of color variations due to a nonuniform film thickness [9]. In such films, convection at voltages high above onset leads to the formation of colored islands, when regions of different thickness are advected with the flow. However, this method provides only qualitative information because many characteristics of the flow dynamics depend on the film thickness. Therefore, homogeneous films are preferable for quantitative measurements. In S_A films of homogeneous thickness, the existence of convective flow can only be detected by measuring the electric current [24] or by means of small dust or smoke particles suspended on the film [9,10]. The velocity of particles advected with the vortices can be determined from the video images. As we have investigated only films of homogeneous thickness, we used the smoke particles to measure small vortex velocities just above the onset of convection. At high vortex velocities, the optical texture in S_C films visualizes the flow field very impressively.

Smectic-*C* films

Following the trajectories of single smoke particles on the video images, we have measured the rotation period of the vortices. Mean values were calculated from rotation periods of at least four different particles for each voltage applied. Results for the smectic-C films are shown in Fig. 4. The

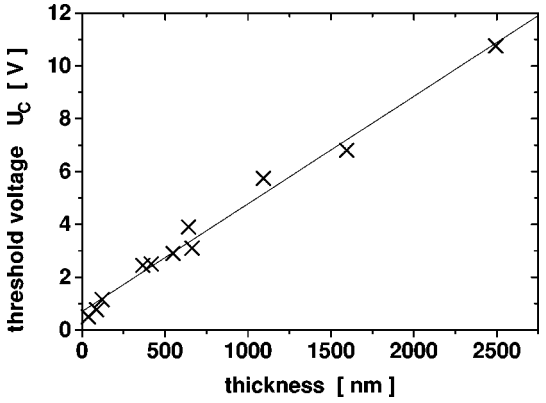

FIG. 5. Thickness dependence of the critical voltage U_c for the smectic-C mixture with a conductivity $\sigma = 8.92 \times 10^{-12}\ \Omega^{-1}\ \mathrm{m}^{-1}$. The solid line is a linear fit $U_c = 0.7\ \mathrm{V} + (4 \times 10^{-3}\ \mathrm{V/nm})s$ to the measured U_c values.

inverse rotation period gives the vortex frequency f_v, which increases with the applied voltage. We assume that the onset of convection is a forward bifurcation where

$$\epsilon = \frac{U^2 - U_c^2}{U_c^2}$$

is the appropriate dimensionless control parameter. The amplitude of the pattern above the bifurcation is expected to be proportional to $\sqrt{\epsilon}$ [10]. A fit of $f_v(U) \propto \sqrt{\epsilon}$ is depicted by the solid line in Fig. 4. The extrapolated intersection of the fitted curve with the zero frequency axis can be used as an approximation for the critical voltage U_c where the convection sets in. If such a fit is performed at voltages near onset, U_c is determined more accurately than by simple visual examination. Note that except for $U \approx U_c$, $\sqrt{\epsilon}$ is similar to a linear function. As very low flow velocities near onset can hardly be measured, a strictly linear relation between f_v and U indicating a transcritical bifurcation cannot be completely ruled out. A possible linear fitting would yield slightly lower threshold voltages.

In the case of our smectic-C films U_c obviously differs from zero and increases linearly with the film thickness s (Fig. 5). This is in qualitative agreement with the results for S_A films presented in [9–11]. Our measurements of the critical voltage showed significantly lower values than those reported in [10] and [11]. From a fit to all our measured results we obtain

$$U_c = 0.7 \pm 0.16\ \mathrm{V} + [(4.0 \pm 0.2) \times 10^{-3}\ \mathrm{V/nm}]s \approx (4 \times 10^{-3}\ \mathrm{V/nm})s.$$

s is the film thickness; the unit is nm (nanometer). Considering a smectic layer thickness of 3.16 nm for 8CB, Mao *et al.* in [11] reported

$$U_c^{\mathrm{Mao}} = \frac{0.332\ \mathrm{mV}}{\mathrm{nm}} s.$$

This difference of about two orders of magnitude can be explained by the very low conductivity of our sample, which was measured by means of dielectric spectroscopy as $\sigma = 8.92 \times 10^{-12}\ \Omega^{-1}\ \mathrm{m}^{-1}$ (at 25 °C). For the measurements reported in [11] by Mao *et al.*, a doped 8CB sample with a higher conductivity $\sigma^{\mathrm{Mao}} = 2 \times 10^{-7}\ \Omega^{-1}\ \mathrm{m}^{-1}$ was used. In the earlier experiments on 8CB films, Morris *et al.* [9,10] measured $\sigma^{\mathrm{Morris}} = 6.6 \times 10^{-8}\ \Omega^{-1}\ \mathrm{m}^{-1}$ and critical voltages equal to U_c^{Mao}. Dayas linear stability analysis [19] predicts a simple formula for the critical voltage:

$$U_c = \frac{s}{\epsilon_0} \sqrt{\sigma \eta R_c}, \tag{5}$$

where η is the viscosity related to shears in the layer plane and $R_c = 76.77$ for Morris wire electrodes, and $R_c = 91.84$ for the case of plate electrodes in the smectic layer plane. Assuming that the basic physical mechanism for the electroconvection in our S_C films is similar to that theoretically investigated in the S_A phase by Daya and co-workers, we expect from Eq. (5) that

$$\left(\frac{U_c \epsilon_0}{s \sqrt{\sigma}} \right)^2 = \eta R_c$$

calculated from our experimental data should be of the same order as the corresponding results for S_A films. Indeed, for our S_C measurements, we obtain $\eta R_c = 141$ kg/ms, while $(\eta R_c)^{\mathrm{Mao}} = 43.3$ kg/ms and $(\eta R_c)^{\mathrm{Morris}} = 131$ kg/ms. As our boundary conditions are a mixture between the ideal wire and plate electrode cases defined by Daya *et al.*, we assume that the R_C constant for our electrode configuration is probably higher than for the wire electrode. The viscosity of the S_C^* mixture at room temperature is also expected to be higher than for 8CB in the S_A phase at the same temperature. If we take into account the uncertainties in the conductivity measurement mentioned in [11] and the different geometrical boundary conditions and viscosities, the measured threshold voltages are in reasonable quantitative agreement with the theory developed in [19] and [20]. We conclude that the vortex flow electroconvection observed in our S_C films is of the same type as the vortex mode reported in [9–11,19,20,24] for S_A films. Elastic torques of the c director obviously play no role for the convective flow.

We note, however, that the viscosity η calculated in this way from the experimental data is considerably larger than typical shear viscosity coefficients of liquid crystals. This was already mentioned in [10] and [11] for the S_A experiments by Morris *et al.* and Mao *et al.* who supposed that the neglect of air drag effects by the theory might explain this discrepancy. However, this assumption has not been verified yet.

The pattern wavelength λ is defined as the lateral periodicity of the flow field (Fig. 3). At voltages near onset, λ is nearly constant, while it shows spatiotemporal fluctuations for higher voltages, especially in the case of low aspect ratios. Therefore the experiments with low aspect ratio are useful for quantitative measurements only in the vicinity of the threshold field U_c. With increasing aspect ratio, the fluctuations of λ become smaller and the vortex pattern becomes nearly stationary even at high voltages. The mean pattern wavelength was estimated by counting the number of vorti-

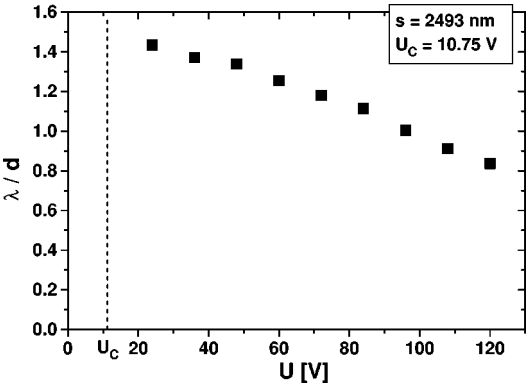

FIG. 6. Change of the vortex pattern wavelength λ scaled with the electrode distance d as a function of the voltage U for a 2593 nm smectic-C film.

ces along the electrode, excluding the vortices at the ends of the electrodes, which are usually bigger as the electric field is inhomogeneous there.

Measured values of the normalized wavelength λ/d are plotted as a function of the applied voltage U (Fig. 6). For dc voltages just above onset, λ is approximately 1.5 times the distance d between the electrodes. This value is similar to Dayas linear stability analysis results for plate electrodes infinitely extended in the x-y plane ($\lambda/d=1.488$). At higher voltages above onset, λ_{dc} decreases to values lower than d. This effect was not observed in Morris experiments on S_A films where the vortex pattern did not change at voltages above onset, until a transition to unsteady flow occurred at high voltages [9]. We assume that these differences are a consequence of the different electrode geometries: While Morris used rigid lateral boundary conditions, we have an open connection to the region outside the electrode gap, which provides a kind of ''free boundary condition'' in the lateral direction. As the vortices at the open ends of our electrode gap can freely expand into the film region outside, a continuous adjustment of wavelength is possible with increasing voltage, while in case of the rigid boundary conditions the pattern retains its metastable onset wavelength. Another difference between our λ measurements and the Morris experiments is that for low frequency ac voltages we did not find any significant variation of λ with frequency in the range between 0 and 1 Hz.

The main difference between S_A and S_C vortex mode electroconvection arises from the existence of the c director and the optical anisotropy of the S_C films. As the dielectric term $\Delta\epsilon\epsilon_0 E^2$ of the free energy density is negligibly small, the c-director orientation is practically free (Goldstone mode). An inhomogeneous flow in the film plane produces a torque on the c director and leads to the formation of walls. In addition, the director field is advected with the flow. This can be used for direct visualization of the flow field, in contrast to S_A films, where the flow in films of homogeneous thickness can be visualized only by the probe particle method. At sufficiently large voltages the walls are wound up to spirals [14], as seen in Fig. 3. The director field is twisted by the unidirectional nonuniform flow field until a steady state is reached where the elastic deformation and flow alignment torques are in balance. Adjacent dark and bright stripes denote 45° change of the c-director orientation.

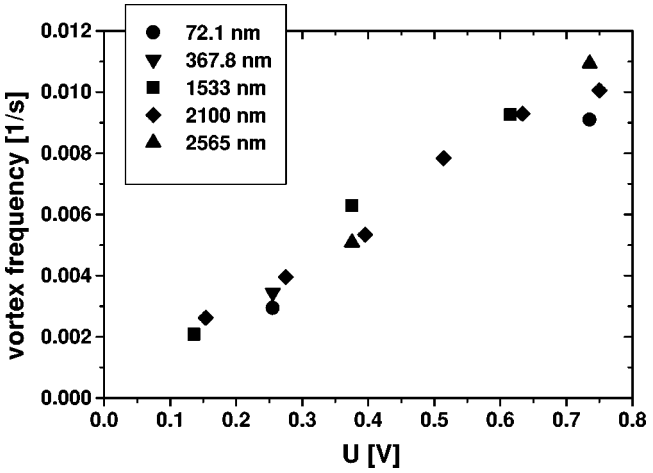

FIG. 7. Measured vortex frequencies for smectic-C^* films of differerent thicknesses ($\sigma=1.3\times10^{-9}\ \Omega^{-1}\ \mathrm{m}^{-1}$). No thickness dependence can be detected. Obviously the threshold voltage is very close to zero.

In case of ac voltages, the vortex flow changes its sign of rotation with the electric field. When the field direction is reversed, the spiral transforms into a ring pattern and is then unwound again. Finally the c-director field winds up in the opposite direction until a new balance is reached.

Smectic-C^* films

In the case of the smectic C^* films investigated, our results for U_c are obviously in contrast to those for nonferroelectric films calculated by Morris *et al.* in [10]. A typical plot for the vortex velocity versus the applied dc voltage is shown in Fig. 7. Even for films thicker than 3μm the extrapolated threshold voltages were practically zero. Moreover, the plots of the vortex frequency against the voltage showed no significant thickness dependence near onset, that is, we cannot detect any critical threshold in the experiments. We assume that the threshold is close to zero, at least much lower than the applied fields. The experiments are compatible with $U_c=0$. This effect cannot be explained by the different conductivity of our S_C^* mixture, which was also measured by means of dielectric spectroscopy. The result $\sigma=1.3\times10^{-9}\ \Omega^{-1}\ \mathrm{m}^{-1}$ was significantly higher than in case of the smectic-C mixture. Using the same ratios as in the smectic-A and -C samples above, we would expect $U_c/s\approx0.048$ V/nm corresponding to $U_c\approx150$ V for a 3μm film, if the same convection mechanism is assumed. Comparing this value with Fig. 7, we conclude that the convection sets in at much lower voltages. A slight thickness dependence of the flow velocity was found at higher voltages: For $U\geqslant5$ V we observed that in thin films ($s<100$ nm) the increase of the vortex velocity with U is higher than in thick films ($s>2\ \mu$m).

Compared to S_A and S_C films, the essential new feature in S_C^* films is the interaction of the spontaneous polarization with the applied electric field. When a dc voltage is applied, the $\mathbf{P}_s$ vector is oriented parallel to the applied electric field. Therefore, the c director is aligned parallel to the electrodes, which can be verified easily with a polarizing microscope by varying the position of the polarizer and the analyzer. There

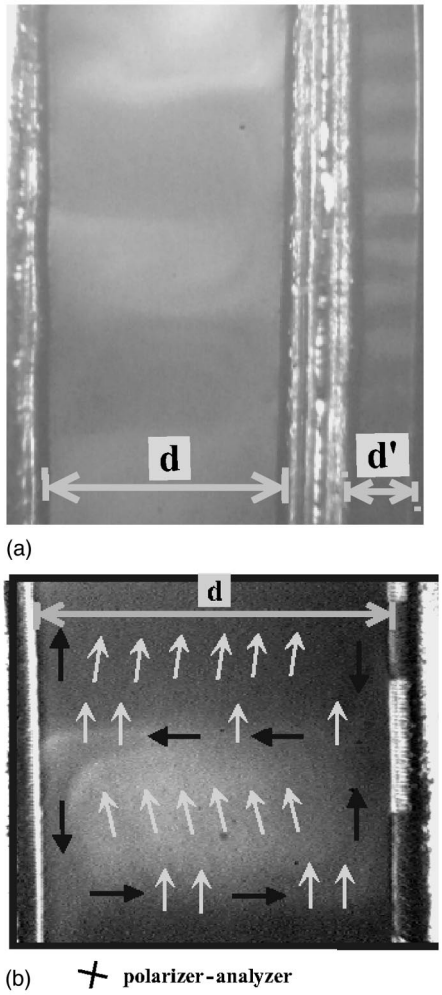

FIG. 8. Electroconvection in smectic-C^* films with dc voltages applied to the electrodes. Vortices rotating in inverse directions produce different brightnesses when polarizers are crossed and a small twist angle between the position of the polarizer and the c director is adjusted. The left image shows electroconvection in a 2100 nm film ($U=60$ V). Note that between the right electrode and the drawing edge of the movable holder, which are adjusted at a distance d', there are convection patterns with a wavelength of the order of d'. The right image shows the convective flow and the orientation of the c director in another film, which has a thickness $s=2565$ nm ($U=60$ V). The c director is oriented nearly parallel to the electrodes due to the coupling of $\mathbf{E}$ and $\mathbf{P}_s$ (arrows as in Fig. 3).

exists practically no critical threshold field for this ferroelectric switching process [25], which is also known as the *polarization Fredericks transition* [8]. An important consequence of the dominating polar interaction and the missing threshold field for the ferroelectric alignment is that the director field in our dc electroconvection experiments always remains nearly fixed. However, due to the torque of the inhomogeneous flow, there is a small deflection of the c director in the sense of the vortex rotation. This allows the visualization of the vortex pattern in S_C^* films with crossed polarizers, when a small twist angle between polarizer and electrode is adjusted. As seen in Fig. 8, vortices rotating in opposite directions produce alternating small director deflections. Consequently, opposite vortices are characterized by different brightnesses in reflectivity.

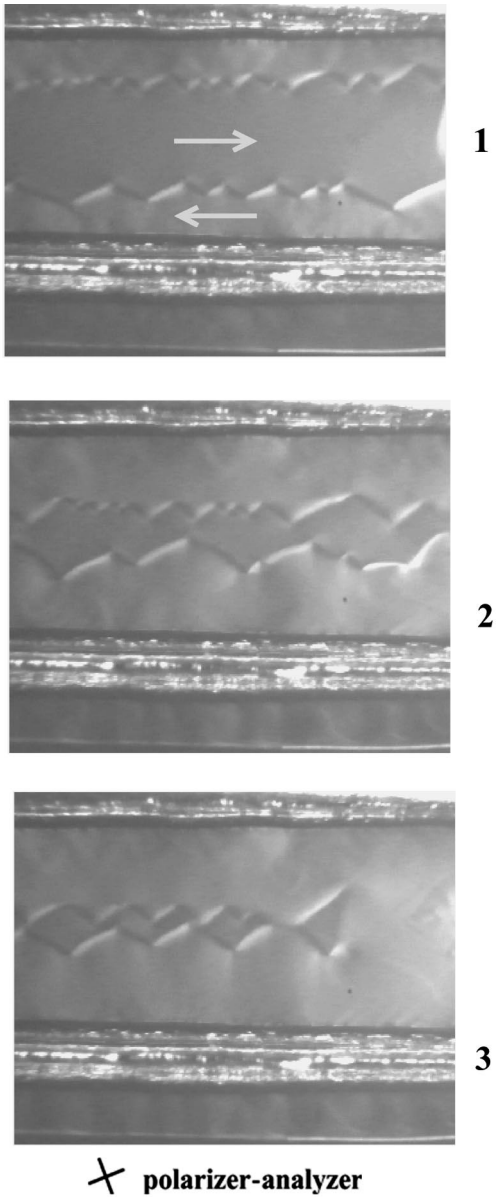

FIG. 9. ''Kink-switching'' in a smectic-C^* film ($s=2100$ nm). Zigzag walls propagate between the electrodes immediately after inverting the sign of the applied ac voltage $U=72$ V at a frequency of 1 Hz. Images 1–3 are taken each after 0.06 s. The arrows indicate the orientation of the c director.

If low frequency ac voltages are applied, the vortices change their rotation sense as in the S_C films. While with dc excitation the pure electroconvection effects can be studied, at ac excitation we observe a superposition of ferroelectric switching and convective flow. When the direction of $\mathbf{E}$ is inverted, the c director performs a 180° reorientation, observed as a change in the optical contrast from dark to bright and back. The inverse switching time linearly depends on the electric field [26]. In the case of perfectly homogeneous films we observed that the switching always starts at the electrodes and solitary switching waves (kinks) appearing as thin zigzag walls propagate to the opposite electrode (Fig. 9). These walls probably separate domains with director orientations differing by 180°. Kink switching was proposed in [27] and [28] as a model to describe dielectric switching in nonferroelectric S_C cells and ferroelectric switching in free-

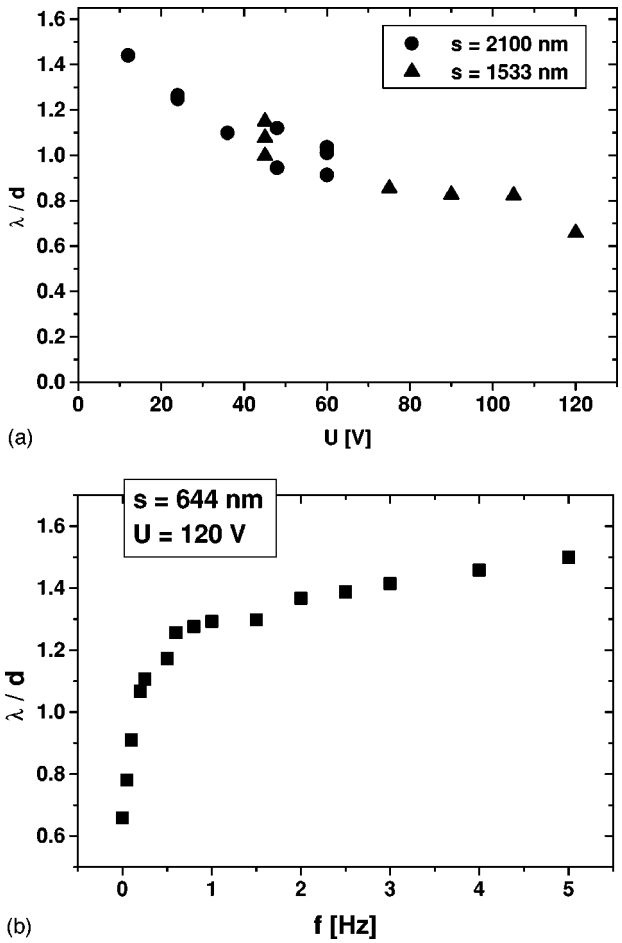

FIG. 10. Change of the vortex pattern wavelength λ scaled with the electrode distance d in smectic-C^* films (a) as a function of the applied dc voltage (b) as a function of the frequency of the applied ac voltage.

standing S_C^* films [28], but has not been observed directly before in free-standing films. The zigzag pattern is an additional interesting feature of the ferroelectric switching process. A reason for the transformation of the kinks into a zigzag pattern is presumably the interaction of $\mathbf{P}_s$ on both sides of the 180° wall. While the wall starts parallel to the electrode, the dipoles favor an orientation of the wall perpendicular to the c director. A detailed analysis is in preparation [29]. At sufficiently high voltages, the switching time is short compared to the ac period and an undisturbed flow evolves after the c-director reorientation.

In the S_C^* films we have also carried out pattern wavelength measurements (Fig. 10). As the vortex pattern is stable even at the highest voltages applied (120 V), λ/d could be measured as a function of U over a large voltage range. Again the dc wavelength decreases significantly with U. A change in the ac pattern wavelength with frequency was found at high voltages, as shown in Fig. 10. At $U=120$ V, λ is only half the estimated dc onset wavelength $[\lambda_{dc}(0)\approx 1.5d]$. When the frequency is increased, the vortex pattern wavelength approaches this onset wavelength again for all voltages. For lower voltages we found that this transition is shifted to lower frequencies. A different frequency dependence was observed in S_A films by Morris *et al.* [10] who measured the critical voltage and the onset wavelength as a function of the frequency between 0 and 5 Hz. The critical voltage was found to increase smoothly with frequency, while the onset wavelength decreased. Above a certain cutoff frequency, the low-frequency vortices were replaced by two opposite lines of smaller vortices along the electrodes. With increasing voltage, λ returned back to the dc onset value. The cutoff frequency is a charge relaxation effect that linearly depends on the inverse electrode distance d^{-1}. As we used a smaller d than Morris *et al.*, and since the ac voltages we applied were always considerably higher than U_c, we did not observe the cutoff in our visual experiments with frequencies below 5 Hz.

Discussion

All experiments we performed on S_C films showed electroconvection of the vortex mode type. This is proved by the fact that the director winds up by more than 180° and that the threshold voltage linearly depends on the film thickness. The formation of CH electroconvection patterns is unlikely in our S_C sample, which has a weakly positive dielectric anisotropy $\Delta\epsilon$. From the theoretical calculations in [8] it follows that for $\Delta\epsilon>0$ and $P_s=0$ no dc Carr-Helfrich instability exists while for $\Delta\epsilon<0$ the threshold is of the order of several volts. An exact calculation of the theoretical threshold is not possible as not all the material parameters required are known for the substance studied in [14]. However, we conclude that in the reported experiments the threshold for the vortex mode was always considerably lower than for any Carr-Helfrich mode. Therefore, the theory that considers only bulk charges is inapplicable for the description of the electroconvection observed in our S_C films and the films studied in [14]. Nevertheless, with changed geometrical boundary conditions and material parameters (conductivity, dielectric anisotropy, viscoelastic constants) the threshold for CH electroconvection can probably be brought below that of the vortex mode. Our experimental results, combined with the theoretical calculations in [8], allow some conclusions concerning a probable crossover between the vortex and a pure CH mode: For dc voltages, such a crossover can be conceived for very thick S_C films with a high conductivity and a negative dielectric anisotropy, as U_c for the vortex mode increases with s while the CH threshold does not depend on the film thickness. On the other hand, a crossover in thick films may also be found for ac voltages, as the vortex mode completely breaks down at high frequencies as the threshold voltage diverges, while the threshold of the dielectric regime due to the Carr-Helfrich electroconvection increases only slightly with f. For sufficiently small electrode distances d, one may also find the conduction regime (and the subharmonic regime for S_C^* films [8]) as the vortex mode cutoff frequency scales only with d^{-1} [10], while the Carr-Helfrich cutoff frequency scales with d^{-2}. This is schematically sketched in Fig. 11. The very low threshold observed in the S_C^* films cannot be explained by the Daya theory. Moreover, as the convection at low voltages shows no thickness dependence (see Fig. 7), the question arises to what extent the surface charge model is applicable for S_C^* films. The missing thickness dependence suggests that mainly bulk charges are involved in the convection mechanism, which therefore might be of the Carr-Helfrich type. In order to es-

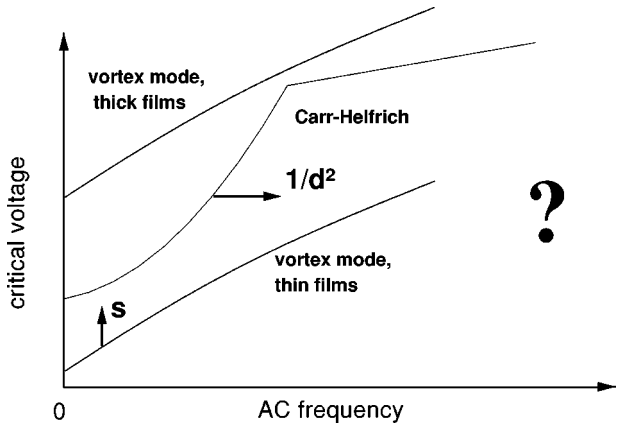

FIG. 11. Possible crossover between Carr-Helfrich mode and vortex mode for smectic-*C* films (schematically sketched). The plot shows the assumed change of the threshold voltage U_c with the frequency of the applied electric field for both modes. Arrows indicate the shift of the vortex mode curve expected when s is changed and the assumed shift of the CH curve expected when d is changed. For a given frequency, the mode with the lowest threshold voltage is expected to be the one which can be observed in experiments.

timate the CH threshold voltage we use an analytical formula given in Appendix B in [8] for the dc convection threshold for ferroelectric films. It predicts that for high spontaneous polarization ($P_s \gg (\pi/d)\sqrt{\epsilon_0 \epsilon_\perp K_1}$) the threshold voltage should decrease with P_s^{-1}, yielding a value of about 6 mV for our S_C^* mixture [30]. These considerations provide evidence that the dc convection mechanism is of the Carr-Helfrich type. The same applies to the observed ac convection patterns in the S_C^* films. At ac excitation, the flow as well as the *c*-director deflection change their signs with the driving field. Therefore we conclude that the charge field is preserved and that we deal with a dielectric CH instability. At high voltages ($U > 5$ V) we suggest that some combined theory of surface and bulk charge mechanisms is necessary to describe the electroconvection in S_C^* films. Such a combined theory would account for the influence of the film thickness mentioned above.

Further experiments will be performed by varying the spontaneous polarization. In the approximation of very low spontaneous polarizations, a crossover between the film thickness independent mechanism observed in the S_C^* mixture and the surface charge driven vortex mode should be expected.

Summary

We have studied electrohydrodynamic convection in S_C and S_C^* films. The in-plane optical anisotropy in both phases allows direct visualization of the flow pattern by polarizing microscopy. In S_C electroconvection, the director field is twisted by the nonuniform flow field. The critical voltages U_c and the vortex rotation velocity as a function of the applied dc voltages were determined. U_c is linearly related to the film thickness s. While effects of convection on the *c*-director field and the optical texture are remarkable, there seems to be no influence of the *c* director on the vortex flow, and the results are well described with the theory developed by Daya *et al.* [19] for S_A films. The pattern wavelength λ is scaling with the electrode distance d and decreases with the applied dc voltage $U > U_c$ both in the S_C and the S_C^* films investigated.

In S_C^* films the *c* director is nearly fixed by the external electric field and the convective flow only leads to deflections of the director field, alternating with the sense of rotation. In contrast to the experiments performed on S_A and S_C films, no film thickness dependence of the flow velocity near onset was found in S_C^* films, and the threshold voltage was below the experimental resolution. These characteristics support the interpretation of the convection mechanism as a Carr-Helfrich instability similar to that predicted by Ried *et al.* [8].

We suggest that a generalized theory for electroconvection in S_C and S_C^* has to include both the Carr-Helfrich mechanism and the vortex mode instability.

ACKNOWLEDGMENTS

The authors are grateful to S. W. Morris (Department of Physics, University of Toronto) for valuable discussions and helpful comments, and to W. Weissflog (Institute of Physical Chemistry, University of Halle) for designing and supplying the smectic-*C* mixture. This work was supported by the DFG (Grant No. STA425/3).

[1] *Pattern Formation in Liquid Crystals*, edited by A. Buka and L. Kramer (Springer, Berlin, 1995).
[2] H. R. Brand, P. E. Cladis, and P. L. Finn, Phys. Rev. A **31**, 361 (1985).
[3] A. B. Davey and W. A. Crossland, Mol. Cryst. Liq. Cryst. Sci. Technol., Sect. A **263**, 2257 (1995).
[4] W. Helfrich, J. Chem. Phys. **51**, 4092 (1969).
[5] G. Hauck and H. D. Koswig, Ferroelectrics **122**, 253 (1991).
[6] P. E. Cladis, P. L. Finn, and H. R. Brand, Phys. Rev. Lett. **75**, 1518 (1995).
[7] J. Maclennan, Europhys. Lett. **13**, 435 (1990).
[8] S. Ried, H. Pleiner, W. Zimmermann, and H. R. Brand, Phys. Rev. E **53**, 6101 (1996).
[9] S. W. Morris, J. R. de Bruyn, and A. D. May, Phys. Rev. Lett. **65**, 2378 (1990).
[10] S. W. Morris, J. R. de Bruyn, and A. D. May, Phys. Rev. A **44**, 8146 (1991).
[11] S. S. Mao, J. R. de Bruyn, and S. W. Morris, Physica A **239**, 189 (1997).
[12] S. Faetti, L. Fronzoni, and P. A. Rolla, J. Chem. Phys. **79**, 5054 (1983).
[13] S. Faetti, L. Fronzoni, and P. A. Rolla, J. Chem. Phys. **79**, 1427 (1983).
[14] A. Becker, S. Ried, R. Stannarius, and H. Stegemeyer, Europhys. Lett. **39**, 257 (1997).
[15] N. Felici, Rev. Gen. Electr. **78**, 717 (1969).

[16] J. C. Lacroix, P. Atten, and E. J. Hopfinger, J. Fluid Mech. **69**, 539 (1975).
[17] P. Atten and J. C. Lacroix, J. Mecan. **18**, 469 (1979).
[18] D. Avsec and M. Luntz, C. R. Hebd. Seances Acad. Sci. **203**, 1140 (1936).
[19] Z. A. Daya, S. W. Morris, and J. R. de Bruyn, Phys. Rev. E **55**, 2682 (1997).
[20] V. B. Deyirmenjian, Z. A. Daya, and S. W. Morris, Phys. Rev. E **56**, 1706 (1997).
[21] MERCK, ZLI-4237-000/-100, preliminary data sheet, E. Merck Darmstadt (unpublished).
[22] I. Kraus *et al.*, Phys. Rev. E **48**, 1916 (1993).
[23] M. Born, *Optik* (Springer, Berlin, 1985).
[24] Z. A. Daya, V. B. Deyirmenjian, S. W. Morris, and J. R. de Bruyn, Phys. Rev. Lett. **80**, 964 (1998).
[25] S. Uto, H. Ohtsuki, M. Teryama, M. Ozaki, and K. Yoshino, Jpn. J. Appl. Phys., Part 2 **35**, L158 (1996).
[26] G. Hauck, H. D. Koswig, and C. Selbmann, Liq. Cryst. **21**, 847 (1996).
[27] P. Schiller, G. Pelzl, and D. Demus, Liq. Cryst. **2**, 21 (1987).
[28] E. I. Demikhov, S. A. Pikin, and E. S. Pikina, Phys. Rev. E **52**, 6250 (1995).
[29] C. Langer and R. Stannarius (unpublished).
[30] In the dimensionless units used in [8] our spontaneous polarization is about 2000. Ried *et al.* present only examples for the small P_s limit in their work, but the equations derived are in principle valid also for high P_s.